

Single phase flow pressure drop and heat transfer in rectangular metallic microchannels



Amirah M. Sahar^a, Mehmed R. Özdemir^a, Ekhlas M. Fayyadh^b, Jan Wissink^a,
Mohamed M. Mahmoud^{a,c,*}, Tassos G. Karayiannis^a

^a School of Engineering and Design, Brunel University, UK

^b Department of Mechanical Engineering, University of Technology, Baghdad, Iraq

^c Faculty of Engineering, Zagazig University, Egypt

ARTICLE INFO

Article history:

Received 21 February 2015

Received in revised form 8 July 2015

Accepted 28 August 2015

Available online 5 September 2015

Keywords:

Single phase flow

Microchannels

Conjugate heat transfer

ABSTRACT

Numerical simulations were performed using Fluent 14.5 to investigate single phase flow and conjugate heat transfer in copper rectangular microchannels. Two different configurations were simulated: (1) single channel with hydraulic diameter of 0.561 mm and (2) multichannel configuration consisting of inlet and outlet manifolds and 25 channels with hydraulic diameter of 0.409 mm. In the single channel configuration, four numerical models were investigated namely, 2D thin-wall, 3D thin-wall (heated from the bottom), 3D thin-wall (three side heated) and 3D full conjugate models. In the multichannel configuration, only 3D full conjugate model was used. The simulation results of the single channel configuration were validated using experimental data of water as a test fluid while the results of the multichannel configuration were validated using experimental data of R134a refrigerant. In the multichannel configuration, flow distribution among the channels was also investigated. The 3D thin-wall model simulation was conducted at thermal boundary conditions similar to those assumed in the experimental data reduction (uniform heat flux) and showed excellent agreement with the experimental data. However, the results of the 3D full conjugate model demonstrated that there is a significant conjugate effect and the heat flux is not uniformly distributed along the channel resulting in significant deviation compared to the experimental data (more than 50%). Also, the results demonstrated that there is a significant difference between the 3D thin-wall and full conjugate models. The simulation of the multichannel configuration with an inlet manifold having gradual decrease in cross sectional area achieved very reasonable uniform flow distribution among the channels which will provide uniform heat transfer rates across the base of the microchannels.

© 2015 The Authors. Published by Elsevier Ltd. This is an open access article under the CC BY license (<http://creativecommons.org/licenses/by/4.0/>).

1. Introduction

Microchannel heat exchangers have several advantages over macro scale ones due to their high surface-to-volume ratio and their small overall volume. The large surface-to-volume ratio leads to high rate of heat transfer and, consequently, makes microchannels excellent tools for compact and ultra-compact heat exchangers. Additionally, the growing interest in micro heat exchangers and their applications especially in cooling high-heat-flux devices such as electronic systems motivated many researchers to

investigate flow phenomena in microchannels. These researchers focused on understanding the characteristics of heat transfer and fluid flow at the micro scale level in order to improve the design and optimize the performance of microchannel heat exchangers.

Studies of single phase flow and heat transfer in microchannels started with the pioneering work of Tuckerman and Pease [1] in which they studied experimentally heat transfer of water flowing under laminar conditions in silicon microchannels. A heat flux value of 790 W/cm² was achieved while the chip temperature was maintained below 110 °C. Many researchers subsequently proceeded to study characteristics of laminar, transitional and turbulent flow in microchannels. One of the main aims of the past experimental studies was to verify whether the conventional theory is applicable at micro scale or new theories need to be developed to

* Corresponding author. School of Engineering and Design, Brunel University, UK.
E-mail address: mohamed.mahmoud@brunel.ac.uk (M.M. Mahmoud).

describe flow in microchannels as reported by Lee et al. [2]. The experimental data in some studies were found to contradict the conventional macro scale theory, see for example [2–4]. However, other studies did not find any size effect on fluid flow and heat transfer in microchannels, [5–8]. The discrepancies reported in the literature can be due to measurement uncertainties and scaling effects as reported by Rosa et al. [9]. They concluded that macro scale theory and correlations are valid at micro scale if measurement uncertainty and scaling effects were carefully considered. These scaling effects include: entrance effects, viscous heating, conjugate heat transfer, electric double layer effects, surface roughness, and properties dependent on temperature, compressibility and rarefactions (for gas flow only).

One of the biggest challenges in multichannel configurations is to achieve uniform flow distribution among the channels, which affects the micro heat exchanger performance as reported by Kandlikar et al. [10]. Hence, most researchers focused on investigating flow distribution in multichannel configurations to obtain an optimal design for micro devices. For example, Tonomura et al. [11] conducted a Computational Fluid Dynamics (CFD) optimization study for the design of a plate-fin micro device consisting of five channels having 0.1×0.1 mm cross sectional area. The simulation was conducted using water as a test fluid. The fluid entered and left the micro device horizontally in a direction normal to the channels (Z-shape). The simulation results indicated that increasing the channel length achieved very uniform flow distribution among the channels particularly at very low flow rates ($Re = 10$). However, when the flow rate was increased further ($Re = 100$), flow mal-distribution was observed. Additionally, the results demonstrated that using an outlet manifold with a cross sectional area as twice as that of the inlet manifold achieved more uniform flow distribution compared to the symmetric manifolds. However, they reported that this will decrease the efficiency of the micro device because using large outlet manifolds increases the “dead volume” inside the micro device and consequently the residence time distribution. In other words, there will be an adverse effect if the microchannel device is used as a micro-reactor. Balaji and Lakshminarayanan [12] modelled a two-dimensional microchannel plate to study the effect of number and location of the inlet and outlet ports on flow distribution along the channels of micro heat exchangers. The dimensions of the microchannel plate were 8.6×7 mm and the width and length of the microchannel were 0.2 and 4 mm, respectively. The depth of the channel was not reported. The flow entered and left the micro heat exchanger vertically from the top surface. It was found that uniform flow distribution can be achieved using either an aligned single inlet and single outlet ports or single inlet port located at the centre line of the micro heat exchanger with two outlet ports located at each corner of the micro heat exchanger. Pan et al. [13] investigated numerically the effects of geometrical parameters such as length, width, manifold area and inlet/outlet port positions on flow uniformity in microchannels plate consisting of ten channels. The inlet/outlet manifold geometry was rectangular. The length and width of the channels were varied from 10 to 50 mm and 0.1 to 0.7 mm, respectively. It was found that the longer microchannel with smaller width resulted in better flow uniformity. Moreover, a relatively uniform velocity could be reached with a large area inlet/outlet manifold and also, when the direction of inlet/outlet ports was perpendicular to the microchannel plane. Therefore, the design of manifolds and microchannels is of considerable importance in micro heat exchanger design.

Most researchers, however, only focused on the optimal design and neglected the effect of axial conduction that leads to non-uniform heat flux in microchannel flow. This is evidenced in the work of Huang et al. [14] who conducted an experimental study

to investigate the effect of axial heat conduction on heat transfer analysis. The parallel microchannel design contained seven microchannels, 40 mm in length, 0.5 mm wide, 0.057 mm deep and a hydraulic diameter of 0.102 mm. The temperature in the axial direction measured at the centre line inside the channel was found to be non-linear for a certain range of Re numbers. Furthermore, the Nusselt number obtained from experimental data varied between 2.55 and 2.58, which is smaller than that predicted by the theoretical model with a constant heat flux boundary condition. These deviations were attributed to axial heat conduction in the experiment.

Performing experiments with microchannels can be very costly in both time and money. To reduce the number of experiments, researchers employ CFD as a tool for heat transfer analysis. CFD can be used in parallel with experimental setups in an effort to predict the flow and heat transfer characteristics of a given surface modification under the specified control parameters and boundary conditions. Computational methods can shorten the design cycle and thereby reduce experimental costs. Fedorov and Viskanta [15] conducted numerical simulations to investigate heat transfer in a three-dimensional asymmetric rectangular microchannel with a range of hydraulic diameters, $D_h = 0.01$ – 0.1 mm and 10 mm channel length. They showed that the 3D simulation is capable of resolving the complex heat flux pattern due to the strong coupling between convection and conduction. Lee et al. [2] performed a numerical study to solve the 3D conjugate heat transfer problem in a microchannel heat sink. The channel hydraulic diameter ranged from 0.318 to 0.903 mm and Reynolds number ranged from 300 to 3500. The numerical simulations were carried out using two different models namely; 3D full conjugate and simplified thin-wall model. In the 3D full conjugate model, they used an arbitrary value of 1.5 mm for the wall thickness. This value was chosen based on the premise that the heat flux is uniformly distributed due to the high thermal conductivity of the substrate. It is worth mentioning here that in the simplified thin-wall model, the axial heat conduction in the wall is neglected. Both approaches showed good agreement with their experimental data, suggesting that the simplified thin-wall model is recommended as a computationally economic alternative for the full conjugate analysis. It is worth noting that they did not take the inlet and outlet manifolds into consideration. Recently, Mansoor et al. [16] performed 3D simulations for flow in a rectangular microchannel incorporating both conduction in the copper substrate and convection by the channel fluid. The microchannel had dimensions of 0.194 mm, 0.884 mm, 25.4 mm for width, height, and length, respectively. The simulations were carried out using the Fluent CFD code. The numerical results were compared with the experimental and numerical results of Lee et al. [2] and were found to be in a good agreement. They found that the average Nusselt number increased with increasing Re . They proposed a correlation for the average Nusselt number as given by Eq. (1), which is valid for $Re = 500$ – 2000 .

$$Nu_{av} = 0.2931 Re^{0.53} Pr^{-0.25} \quad (1)$$

In this paper, two different configurations were simulated; a single channel and a multichannel configuration. The focus in this study is to examine the accuracy of numerical schemes through comparing the predicted friction factor and Nusselt number with experimental data and conventional theory. In both configurations, the conjugate effects on heat transfer were considered. The flow distribution among the channels was the focus of the work carried out in the multi-microchannel configuration.

2. Experimental setup

Two experimental systems were used to validate the numerical results in the present study. The two systems were designed to conduct single and two phase flow boiling in microchannels. The first one was designed for flow boiling of water in single microchannels while the second was designed for flow boiling of refrigerants in multi-microchannel configurations. Detailed description is given in Refs. [17,18] and a brief summary of each system is given below.

2.1. Water test rig – single channel facility

The experimental facility used to study water flow in a single channel is depicted in Fig. 1 from Ref. [17]. It consists of a reservoir, sub-cooler, gear pump with a programmable variable speed drive, Coriolis flow meter, pre-heater, test section, inline filters and condenser. A water-glycol circulation chiller is used to meet the cooling load at the condenser and sub-cooler. De-ionized water was used as a test fluid. After de-gassing in the reservoir, water was circulated through the system and its temperature was controlled at the test section inlet through a PID controller. The test section was made of an oxygen-free copper block (12 mm wide \times 25 mm high \times 72 mm long). A single rectangular microchannel 0.39 mm high, 1 mm wide and 62 mm long was cut in the top surface of the block using a Kern HSPC 2216 high-speed micro-milling machine. The measurements were accurate to $\pm 2 \mu\text{m}$ giving a mean uncertainty of $\pm 0.34\%$ for the hydraulic diameter which is 0.56 mm. The average surface roughness R_a of the channel base was measured using a Zygo NewView 5000 surface profiler with an accuracy of $\pm 1 \text{ nm}$. The R_a value was found to be 0.392 μm near inlet, 0.242 μm near middle and 0.330 μm near outlet.

The test section was heated using one cartridge heater embedded below and parallel to the channel length. Water inlet and outlet temperature was measured using K-type thermocouples while the axial channel bottom surface temperature was measured using six K-type thermocouples located 1.5 mm below the channel bottom. Six differential pressure sensors Honeywell 26PCC were used to measure the local pressure between the channel inlet and outlet. All data were recorded using NI-compact modular data acquisition system with Labview program.

2.2. Refrigerant test rig – multichannel facility

The schematic drawing of this rig is depicted in Fig. 2 from Ref. [18]. It consists of R134a reservoir, gear pump, sub-cooler, two Coriolis flow meters (for low and high mass flow range), pre-heater, test section, inline filters and condenser. The system pressure was controlled through controlling the reservoir temperature using an immersion heater and a PID controller. Secondary cooling loop, not shown in Fig. 2, was used to meet the cooling load at the subcooler and condenser. The fluid temperature at the test section inlet was controlled through the preheater and sub-cooler. A sight glass was inserted before the test section inlet to make sure that there are no bubbles entering the test section. All measurements were recorded using IMP data acquisition system model 35951C and a Labview program.

The test section details are depicted in Fig. 3 from Ref. [18]. It consisted of: (1) twenty five microchannels cut on the top surface of an oxygen free copper block, (2) polycarbonate housing, (3) quartz glass top cover plate to allow flow visualization, (4) cartridge heaters. The dimensions of the copper block were 15 mm width, 20 mm length and 74 mm height. The microchannels were cut using a CNC machine with a feed rate of 550 mm/min. The nominal dimensions of the microchannel were 0.3 mm width, 0.7 mm depth, 0.2 mm fin thickness (thickness of the wall between channels) and 20 mm length. The surface roughness of the bottom wall was measured using Zygo NewView 5000 surface profiler and the measured R_a value was 0.301 μm . The dimensions of the channels were subsequently measured using an electron microscope and the values were 0.297 mm for width, 0.697 mm for height and 0.209 mm for the fin thickness. Three cartridge heaters (200 W each) were inserted at the bottom of the copper block to provide the heating power for the test section. Six thermocouples (type-T) were inserted at the vertical centre line of the copper block with 12 mm equidistant intervals to measure the heat flux. Three thermocouples were inserted at 1 mm below the microchannel bottom and spaced by 8 mm in the axial direction for heat transfer measurements; i.e. local heat transfer in the axial direction. All thermocouples were calibrated with an accuracy of $\pm 0.3 \text{ K}$. The housing consisted of plenum and manifold with the inlet and outlet plenums deeper than inlet and outlet manifolds as seen Fig. 3, [18]. The fluid inlet and outlet temperature were measured using T-type

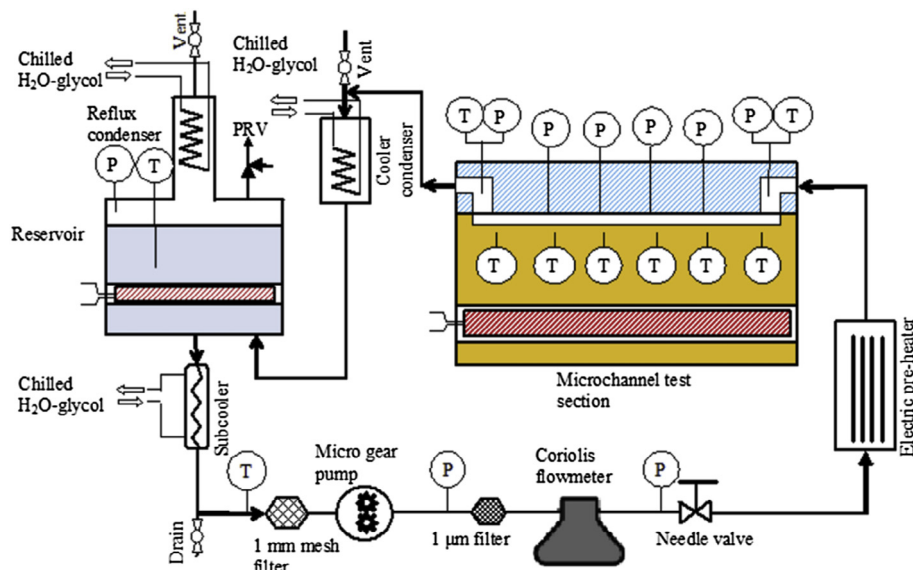


Fig. 1. Schematic of water experimental facility [17].

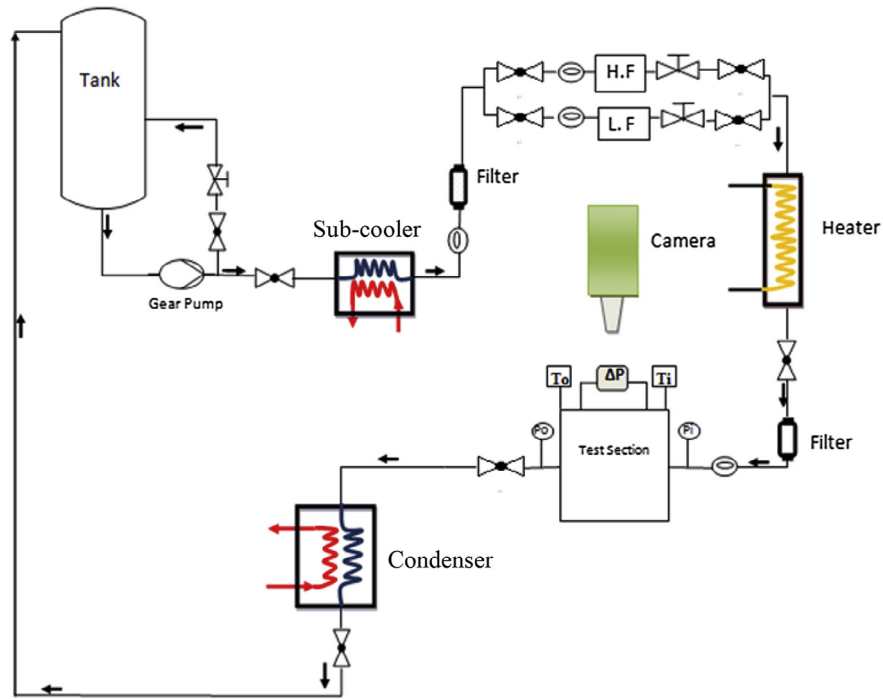


Fig. 2. Schematic of refrigerant experimental facility [18].

thermocouples inserted into the plenum and calibrated with an accuracy of ± 0.5 K. The fluid inlet and outlet pressures were measured using absolute pressure transducers, which were calibrated with an accuracy of $\pm 0.15\%$ and $\pm 0.32\%$, respectively. Pressure drop across

the test section was measured directly using calibrated differential pressure transducer with an accuracy of $\pm 0.081\%$.

3. Data reduction

3.1. Pressure drop

The pressure drop along the microchannels is given by:

$$\Delta P_{ch} = \Delta P_{meas} - \Delta P_{loss} \tag{2}$$

3.1.1. Single channel

For the single channel configuration, the pressure loss ΔP_{loss} which is defined by Eq. (3) below includes the pressure loss due to the inlet and outlet manifolds and the sudden contraction and enlargement. In our case, the flow enters and leaves the channel in a direction normal to the channel axis, see Fig. 4 presented later.

$$\Delta P_{loss} = 2 \left(\frac{1}{2} \rho_f V_p^2 K_{90} \right) + \frac{1}{2} \rho_f V_{ch}^2 (K_c + K_e) \tag{3}$$

where ρ_f is the fluid density, V_p and V_{ch} are the velocity in the manifold and inside the channel respectively, K_{90} is the pressure loss coefficient, K_c and K_e are the sudden contraction and enlargement coefficients, respectively. The values of these coefficients can be

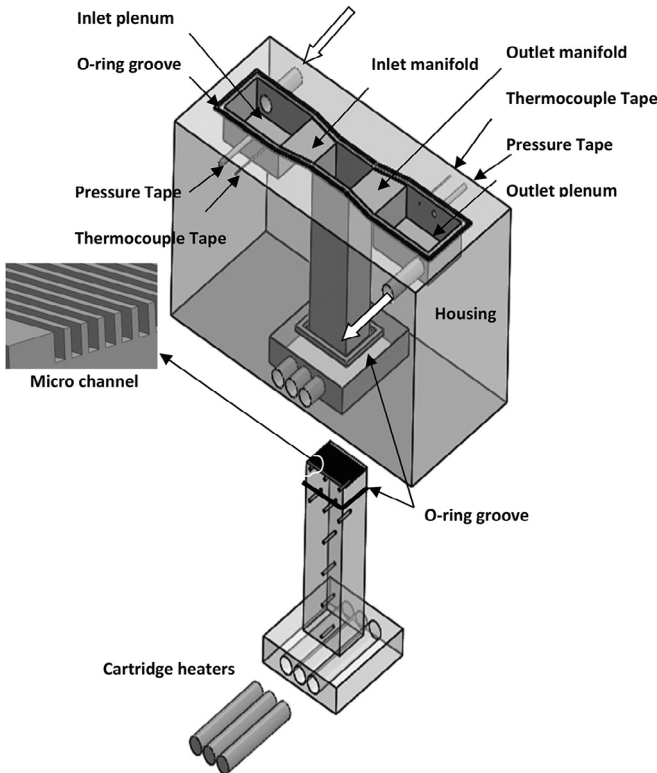


Fig. 3. Details of the test section used in the experiments of [18].

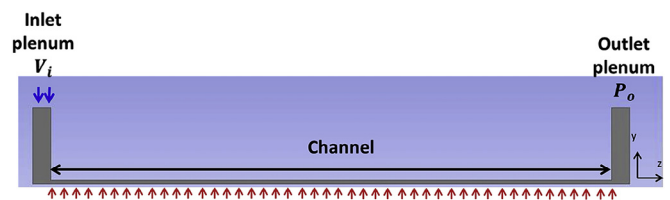


Fig. 4. 2D computational domain of single microchannel system (Model 1).

found in Ref. [19]. The estimated average value of the minor pressure loss components in Eq. (3) are: (1) the pressure loss due to the inlet and outlet manifolds represents 0.38% of the total measured pressure drop, (2) the pressure loss due to the sudden contraction represents 6.4% of the total measured pressure drop, (3) the pressure loss due to sudden enlargement represents 8.7% of the total measured pressure loss. Thus, the pressure drop across the channel represents 84.52% of the total measured pressure drop.

3.1.2. Multichannel

For the multichannel configuration, the flow enters the channels through an inlet manifold with a gradually reducing cross sectional flow area and leaves the channels through a manifold, which has a gradually increasing cross sectional flow area as depicted in Fig. 3. Thus the pressure loss term ΔP_{loss} in Eq. (2) is given by:

$$\Delta P_{loss} = \Delta P_{im} + \Delta P_c + \Delta P_e + \Delta P_{om} \quad (4)$$

where ΔP_{im} and ΔP_{om} are the pressure loss across the inlet and outlet manifolds, respectively. These losses are given by the following equations, see Ref. [20].

$$\Delta P_{im} = [1 - \sigma^2 + K_{im}] \times \frac{1}{2} G^2 v_f \quad (5)$$

$$\Delta P_{om} = - \left[\frac{1}{\sigma^2} - 1 + K_{om} \right] \times \frac{1}{2} G^2 v_f \quad (6)$$

The loss coefficients K_{im} and K_{om} depend on the manifold convergence and divergence angle θ and the values are summarized in Ref. [21] in a table form as a function of the area ratio and angle θ . The values are 0.134 for K_{im} and 0.11 for K_{om} for our design. In the above equations σ is the small to large cross sectional area ratio. The sudden contraction and enlargement in Eq. (4) are given by the following equations, see Ref. [20]:

$$\Delta P_e = - \left[\frac{1}{\sigma^2} - 1 + (1 - \sigma)^2 \right] \times \frac{1}{2} G^2 v_f \quad (7)$$

$$\Delta P_c = [1 - \sigma^2 + 0.5(1 - \sigma)] \times \frac{1}{2} G^2 v_f \quad (8)$$

The Fanning friction factor can then be calculated using Eq. (9) for both the single and multichannel arrangement as:

$$f = \frac{\Delta p_{ch} D_h}{2 L_{ch} \rho_f V_{ch}^2} \quad (9)$$

where the hydraulic diameter is defined as:

$$D_h = \frac{4 W_{ch} H_{ch}}{2(W_{ch} + H_{ch})} \quad (10)$$

The Reynolds number is defined as:

$$Re = \frac{\rho_f V_{ch} D_h}{\mu_f} \quad (11)$$

3.2. Heat transfer rates

For the single channel configuration, the rate of heat loss from the test section to the ambient was determined experimentally using

an energy balance and was found to be approximately 5.2–9.2% of the input electrical power at the cartridge heater. The rate of heat removal q_{rem} by the working fluid is given as:

$$q_{rem} = P - q_{loss} = \dot{m} c_p (T_o - T_i) \quad (12)$$

where P is equal to the product of the measured voltage and current supplied to the cartridge heater. For the multichannel configuration, the base heat flux q_b was calculated from the measured temperature gradient in the vertical direction ($q_b = k_w dT/dy$). The average heat flux is then calculated by the following equation:

$$q'' = \begin{cases} \frac{q_{rem}}{A_{ht}} & \text{single channel} \\ \frac{q_b W}{N(W_{ch} + 2H_{ch})} & \text{multichannel} \end{cases} \quad (13)$$

$$A_{ht} = (W_{ch} \times 2H_{ch}) L_{ch} \quad (14)$$

The average experimental heat transfer coefficient is given by:

$$h_{av,exp} = \frac{q''}{\Delta T_{lm}} \quad (15)$$

and for both the single and multichannel arrangement the log-mean temperature difference approach is used due to the possible linear increasing temperature at constant heat flux:

$$\Delta T_{lm} = \frac{T_o - T_i}{\ln \left(\frac{(T_w - T_i)}{(T_w - T_o)} \right)} \quad (16)$$

The corresponding average Nusselt number is then calculated as:

$$Nu_{av,exp} = \frac{h_{av,exp} D_h}{k_f} \quad (17)$$

The propagated uncertainty in the measured friction factor and heat transfer coefficient was calculated according to the method described in Coleman and Steele [22] and the average values were 10.2% and 6.3% respectively.

4. Numerical analysis

4.1. Description of models

4.1.1. Single-channel configuration

Numerical simulations were performed to solve the conjugate heat transfer problem in a microchannel, accounting for both convection in the channel and conduction in the copper substrate. Four approaches, listed below, were used in the single channel configuration to examine the accuracy of different numerical schemes (2D versus 3D) through comparing the predicted friction factor and Nusselt number with experimental data and conventional theory.

1. Model 1: the geometry used in this model is depicted in Fig. 4 where 2D simulation was conducted under constant heat flux boundary condition applied at the bottom surface of the channel only while the top surface was adiabatic.
2. Model 2: the geometry used in this model is depicted in Fig. 5. In this model, 3D thin-wall approach was adopted with wall thickness is zero (no axial conduction). The constant heat flux boundary condition was applied at the bottom surface only while the other three walls were considered adiabatic. This model is

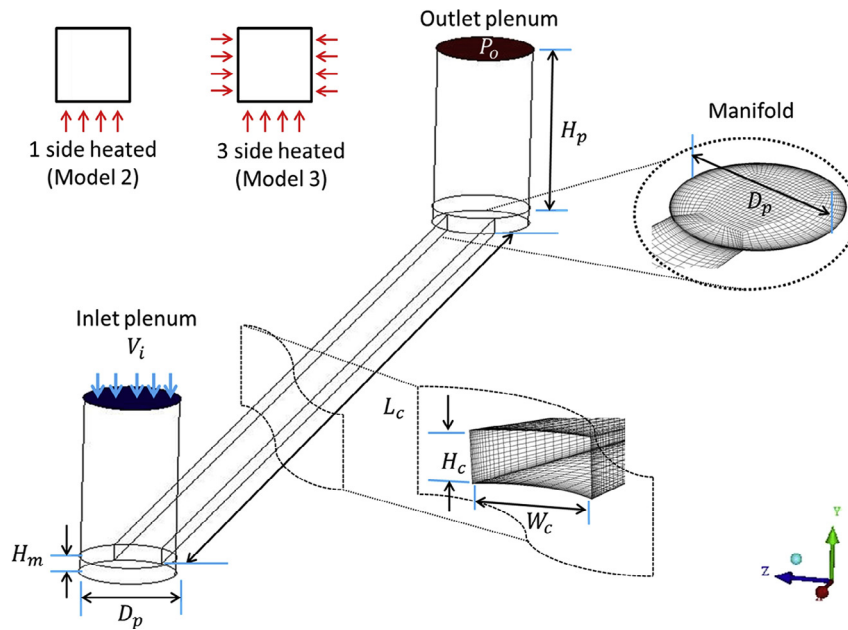


Fig. 5. Computational domain of single microchannel system (Thin-wall Models 2 and 3).

called herein this paper as 3D thin-wall one side heated as seen in Fig. 5 (the top left corner). In the thin-wall model, the thermal boundary conditions are applied at the outer surface of the wall (at the solid-fluid interface), see Ref. [23] for more details.

3. Model 3: this model is similar to Model 2 except that the constant heat flux boundary condition was applied at the bottom and the two side walls while the top wall was kept adiabatic. This model is called herein 3D thin-wall three sides heated as seen in Fig. 5 (the top left corner).
4. Model 4: the geometry used in this model is depicted in Fig. 6 where 3D full conjugated model was simulated. In this model, the full copper block similar to the one used in the experiment was simulated. A constant heat flux boundary condition was applied at the location of the cartridge heater.

4.1.2. Multichannel configurations

The multichannel system was simulated using the 3D full conjugated model similar to Model 4 in single channel system as seen in Fig. 7 and is called Model 5. This model is exactly similar to the experiment excluding the inlet and outlet plenums. The dimensions of the channels are shown in Fig. 8.

4.2. Numerical method

A CFD analysis was carried out to investigate the characteristics of fluid flow and conjugate heat transfer in microchannels. The following assumptions were adopted:

1. Steady state fluid flow and heat transfer.
2. Incompressible fluid

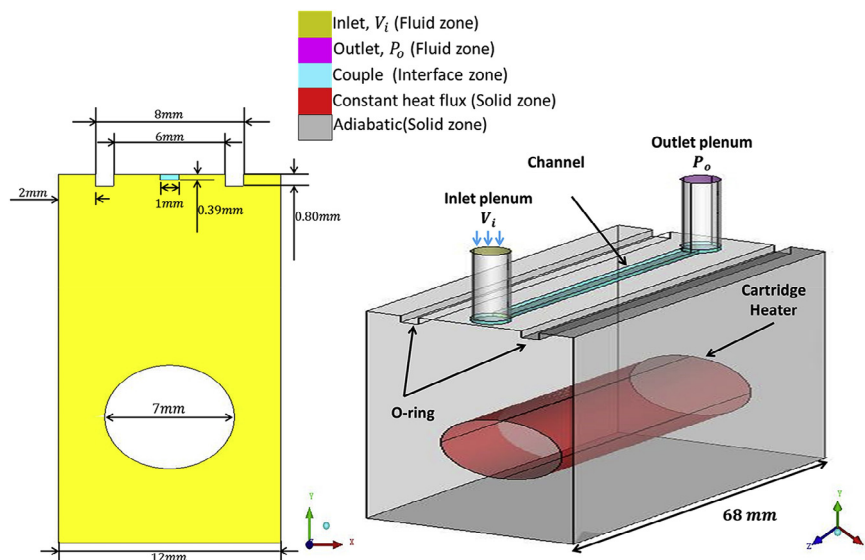


Fig. 6. 3D fully conjugated computational model of single microchannel system (Model 4).

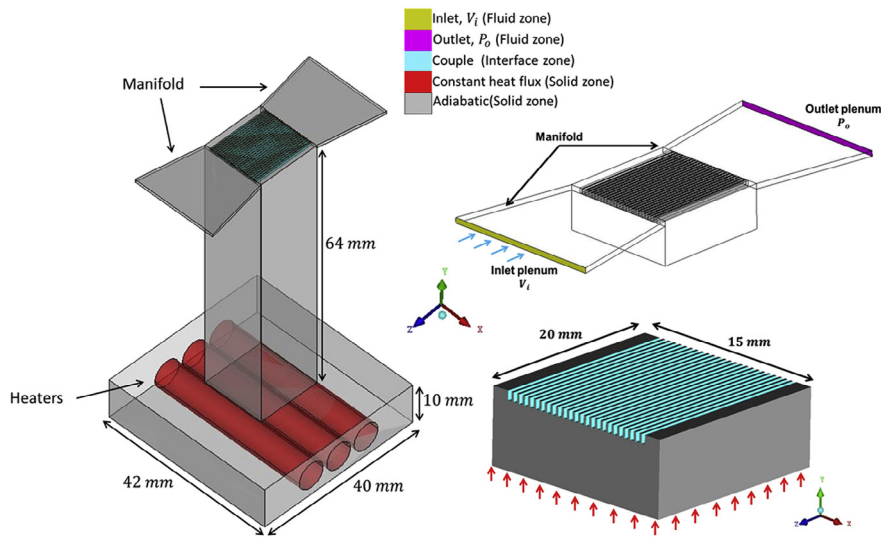


Fig. 7. 3D fully conjugated computational model of multi-microchannel system (Model 5).

3. Negligible radiative heat transfer
4. Constant solid and fluid properties

Based on the above assumptions, the governing differential equations used to describe the fluid flow and heat transfer in the microchannel are given as:

Conservation of mass (continuity)

$$\nabla(\rho\vec{V})=0 \quad (18)$$

Conservation of momentum

$$\vec{V} \cdot \nabla(\rho\vec{V}) = -\nabla p + \nabla \cdot (\mu \nabla \vec{V}) \quad (19)$$

Conservation of energy for fluid

$$\vec{V} \cdot \nabla(\rho c_p T_f) = \nabla \cdot (k_f \nabla T_f) \quad (20)$$

Conservation of energy for solid

$$\nabla \cdot (k_w \nabla T_w) = 0 \quad (21)$$

A number of uniform inlet velocities were selected in order to match the Reynolds number values obtained in the experiment. At

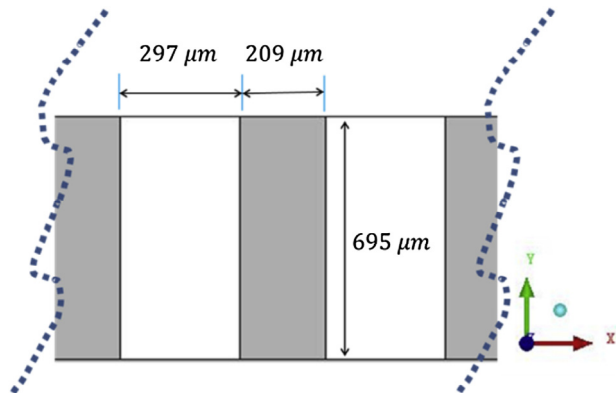


Fig. 8. Channel cross-section domain (Multichannel system).

the outlet a pressure outflow boundary condition was employed. The no slip boundary condition was assigned for all wall boundaries. The heat loss through the top cover was considered to be negligible. In the thin wall approach (Model 2 and Model 3) adiabatic conditions were employed at the top wall while along the bottom (and also the side walls for the 3D simulation) a constant heat flux q'' was applied. For the 3D full conjugate analysis (Model 4 and Model 5), the continuity of the temperature and heat flux is used as the conjugate boundary condition to couple the energy equations at the fluid and solid interface.

The computations were performed using the commercial software package FLUENT 14.5. ICEM 14.5 was utilized for the geometry construction and mesh generation. The viscous laminar model or standard k- Ω model was used for laminar ($Re < 2000$) and turbulent ($Re > 2200$) flow, respectively. The SIMPLE scheme is used to resolve the pressure-velocity coupling. The flow momentum and energy equations are solved with a first-order upwind scheme. The simulations are performed using a convergence criterion of 10^{-6} . The hexa meshing grid scheme was used to mesh the system. A highly compressed non-uniform grid near the channel walls was adopted in order to properly resolve viscous shear layers. Grid nodes were also concentrated along the axial direction in the entrance of the channel in order to properly resolve the flow and thermal development regions as adopted by Fedorov and Viskanta [15] and Qu and Mudawar [24]. A grid dependency study was conducted in a single channel system at the highest and lowest Re number, using the friction factor as a criterion to ensure the results are independent of the mesh. It was carried out in 3D model (thin wall Model 3) by varying the number of grids in the microchannel. Three different grid sizes of $20 \times 15 \times 300$, $20 \times 15 \times 600$ and $20 \times 50 \times 600$ were used for x-y-z direction representing width, height and length, respectively. Grid sensitivity study was conducted in both laminar and turbulent region. In laminar region, predicted friction factor changed by less than 1% from the $20 \times 15 \times 300$ to the $20 \times 50 \times 600$ grid size. While in turbulent region, the predicted friction factor changed by 3.5% from the first to second grid, and only 1% upon further refinement to the finest grid. Hence the intermediate grid size of $20 \times 15 \times 300$ was chosen in order to save computational time. In the multichannel system (Model 5), average velocities in the microchannels are compared in Fig. 9 for six different grid sizes to investigate the effect of grid sensitivity. The

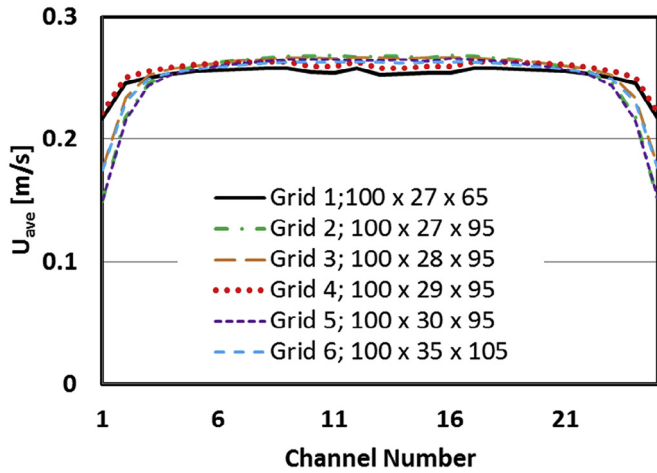


Fig. 9. Effect of grid size on average velocity in microchannels in multichannel system.

average velocity distributions were found to slightly change from grid 1 to 6. Based on the results shown in Fig. 9, computational grid 5 was employed for multichannel configurations in this study.

4.3. Data analysis

The local heat transfer coefficient is defined as:

$$h(x) = \frac{q''(x)}{T_{w,av} - T_{f,av}} \quad (22)$$

These temperatures were the average of five locations along the channel width at each axial distance. The local Nusselt number is defined as:

$$Nu(x) = \frac{h(x)D_h}{k_f} \quad (23)$$

The average heat transfer coefficient is defined as:

$$h_{av,num} = \frac{1}{L_{ch}} \int_0^{L_{ch}} h(x) dx \quad (24)$$

$$Nu_{av,num} = \frac{h_{av,num}D_h}{k_f} \quad (25)$$

5. Results and discussions

5.1. Single channel configuration

The predicted numerical friction factor results were verified using current experimental data and the Shah and London [19] correlations for developed and developing laminar flow and the Blasius [25] equation for turbulent flow as seen in Fig. 10. The figure depicts the validation of the friction factor predicted by the 2D and 3D models. It indicates that the 2D model underpredicts the values by about 30% while the 3D model agrees very well with the experimental data. This could be attributed to the reduction in wall shear stress arising from ignoring the channel side walls in the 2D simulation. Additionally, it is obvious that both 3D model and experimental data exhibit a transition change at $Re \approx 1600$. In other words, the early transition reported by some researchers ($Re < 1000$) was not observed in the present study,

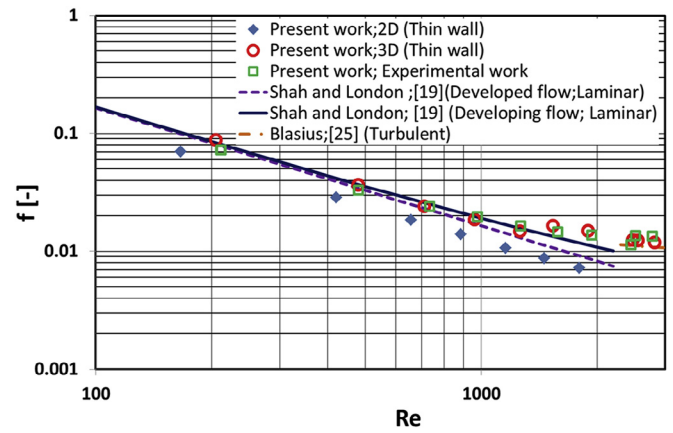


Fig. 10. Comparison of predicted friction factor with existing experimental results and existing correlations.

which agrees with Harms et al. [5] and Zhang et al. [26]. Harms et al. [5] investigated water flow in a rectangular microchannel ($D_h = 401 \mu m$) and found that the transition occurs at $Re \approx 1500$. Recently, Zhang, et al. [26] studied flow and heat transfer characteristics of six rectangular microchannels with D_h ranging from 0.48 mm to 0.84 mm. The experimental results indicated that the laminar to turbulent transition occurs at $Re = 1200-1600$. Researchers who reported early transition thought that it occurs due to channel size reduction as reported by Peng et al. [27] and Pfund et al. [28].

Fig. 11 presents a comparison of the computationally predicted average Nusselt number (Eq. (25)) in the laminar and turbulent regions with experimental data (Eq. (17)) and correlations [19,34,35]. The figure shows that the 2D thin wall model (Model 1) agrees very well with Shah and London [19] for developing laminar flow but highly under-predicts the experimental values. This could be due to the fact that Shah and London solved the 2D problem. It is worth mentioning that the experimental data presented in this figure were calculated based on the assumption of uniform and constant heat flux boundary condition. In order to validate the numerical method, 3D thin-wall models were simulated using the same assumption as the experimental data reduction (uniform and constant heat flux) and the results are shown in Fig. 11. The figure shows that the 3D

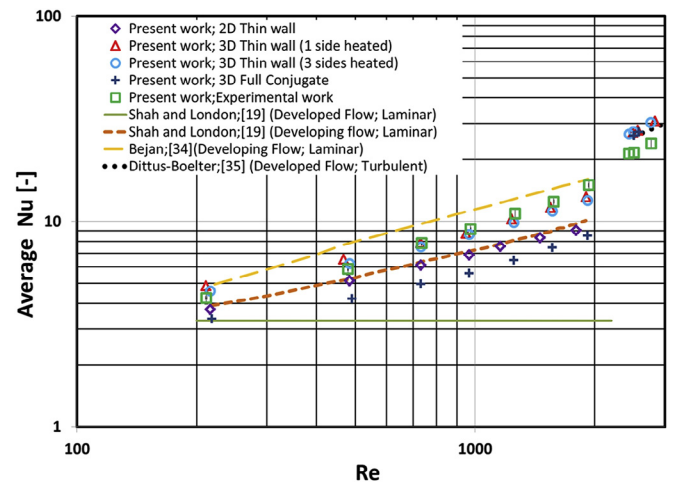


Fig. 11. Comparison of predicted average Nusselt number with experimental data and correlations.

thin-wall models (Models 2 and 3) exhibit excellent agreement with the experimental values and the insignificant difference between the two models could be due to the short height of the channel (0.39 mm). The excellent agreement of the thin-wall models with the experimental data arises from the similarity in the assumption of uniform constant heat flux, which may be true or may not as will be discussed later. On the contrary, the 3D full conjugated model Model 4 (simulating the experiment) demonstrated significant deviation, see Fig. 11. This deviation may be attributed to the conjugate effect, i.e. heat flux is not uniformly distributed along the channel. Iaccarino et al. [29] reported that the conjugate effects should be taken into consideration. To clarify this point, the local heat flux along the channel predicted using the 3D full conjugate model was plotted in Fig. 12 for the bottom and side walls.

The local heat flux is defined as $q'' = k_f \Delta T / \Delta y$. The figure demonstrates that the heat flux is very high near the entry region due to the thin thermal boundary layer and then it decreases continuously along the channel. Thus, the average Nusselt number is expected to be lower than the thin-wall models in which the heat flux is assumed constant. The high heat flux in the entry region was also found by Qu and Mudawar [24] and Tiselj et al. [30]. As illustrated in Fig. 12, the heat flux varies in the cross-stream direction where the heat flux at the bottom wall was found to be higher compared to that at the side walls. This is due to the fact the near-wall flow velocity in the middle of the bottom wall is larger than in the middle of the (smaller) side walls. A higher near-wall velocity results in an increased (wall-averaged) heat transfer rate.

Figs. 13 and 14 depict the fluid and channel bottom wall temperature along the channel length for the 3D thin-wall approach three side heated Model 3 (see Fig. 13) and the 3D conjugate heat transfer approach Model 4 (see Fig. 14(a)) and Model 5 (see Fig. 14(b)) at $Re = 218$ and $Re = 585$, respectively. It is worth mentioning that in the thin wall approach uniform heat flux (at the bottom and side walls) boundary condition was assumed. In the full conjugated heat transfer approach, the full copper block with the embedded cartridge heater was simulated, which is exactly the same as the experiment. As seen in Fig. 13 and as expected from the theory for constant heat flux boundary condition, the fluid and wall temperature increase linearly in the fully developed region. This trend is expected to occur because the wall thickness was assumed to be zero, i.e. there is no conjugate effect. On the contrary, Fig. 14(a) demonstrates a very clear conjugate effect where the change in the wall and fluid temperatures is not linear although constant heat flux boundary condition was assumed at the location of the cartridge

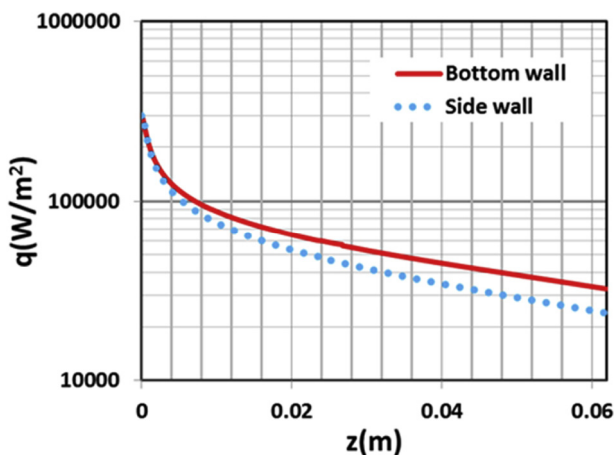


Fig. 12. Prediction local heat flux distribution for bottom and side wall along the channel length (Model 4).

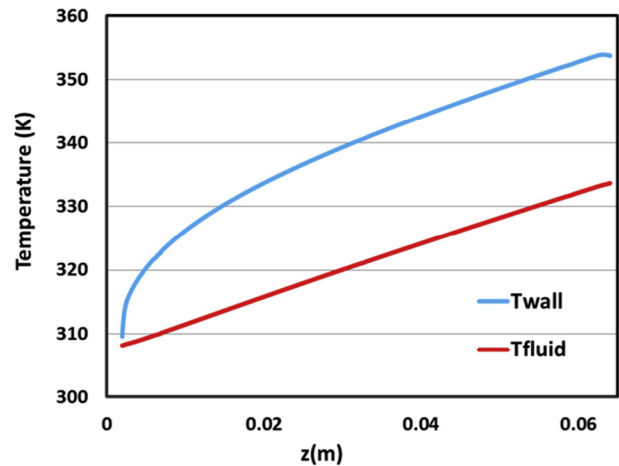


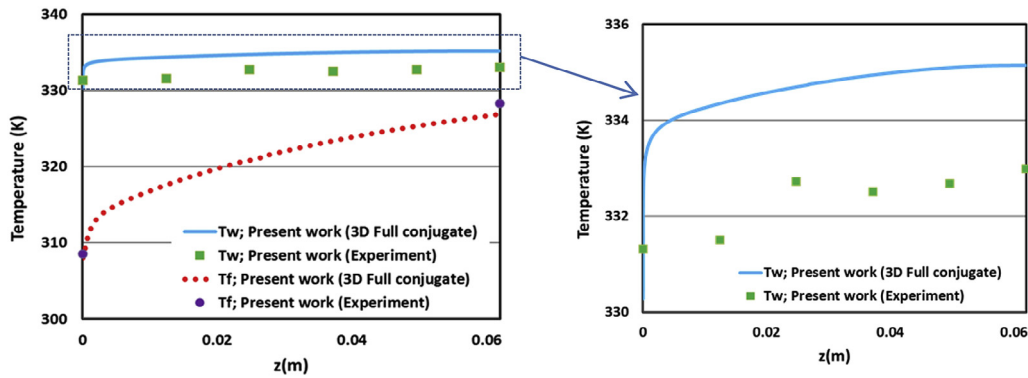
Fig. 13. Axial temperature variation of fluid and bottom wall along the channel at $Re = 216$ (Thin wall analysis).

heater, see Fig. 6. The high thermal conductivity of copper makes the heat transfer problem multi-dimension and consequently the wall temperature approaches from the isothermal conditions. The wall temperature measured at six axial locations is also included in Fig. 14(a). The measured values were corrected using 1D heat conduction to consider the 1.5 mm distance between the thermocouple and channel base. As seen in the figure, the simulation predicts almost similar trend as the experiment but with slightly higher values. The same behaviour was found for the multichannel system as illustrated in Fig. 14(b).

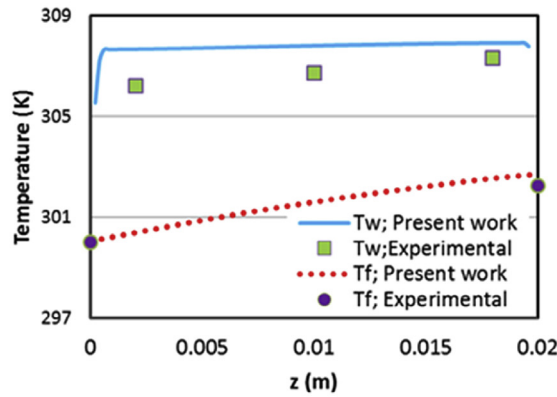
Fig. 15 presents the local Nusselt number versus axial distance for the four models at $Re = 216$. It is clearly shown that Nu predicted by Model 1 (2D model) and Models 2 and 3 (3D thin-wall models) approaches a fully developed constant values of 2.37 and 3.34, respectively. On the contrary, the Nu predicted by the 3D full conjugated model (Model 4) decreases continuously with axial distance. This confirms that the boundary condition at the channel walls is not a constant heat flux as previously discussed in Fig. 12. Comparing the 2D and 3D thin wall simulation results in Figs. 10 and 11, it can be seen that the predicted friction factor and local Nusselt number in the 2D simulation are lower than in the 3D simulation. This is due to the presence of side-walls in the 3D simulation that give rise to cross-stream fluid motions resulting in higher values for both f and Nu .

The numerical results found in this study agree with the findings of Moharana et al. [31]. They conducted a numerical study on simultaneously developing flow under conjugate conditions in a square microchannel. They studied the effect of substrate thickness and thermal conductivity on heat transfer characteristics. They found that, the local heat flux becomes uniformly distributed along the channel after the entry region when the substrate thickness becomes very small (thin wall approach in the present study) or when the substrate thermal conductivity becomes very low. In this case, they found that the wall and fluid temperatures increase linearly as also found in the current study, see Fig. 13. When the substrate thickness and thermal conductivity was high (fully conjugated model in the present study), the heat flux was found to decrease with axial distance, similar to what is depicted in Fig. 15.

It is worth mentioning that Lee et al. [2] did not find a significant difference between the thin-wall and full conjugate models in their numerical study. Thus they recommended using the thin-wall approach for simulating heat transfer in microchannels. This result seems contradicting to the results of the present study and



(a)



(b)

Fig. 14. Axial temperature variation of fluid and bottom wall along the channel (a) single channel system at $Re = 216$, (b) multichannel system at $Re = 585$ (3D fully conjugated analysis).

need a comment. The insignificant difference between the two models reported by Ref. [2] could be due to the fact that the substrate thickness in their study was too small (1.5 mm). This could be valid for simulating thin test sections that incorporate integrated heaters. On the contrary, the design investigated in the present study use a large copper block with embedded cartridge heaters which may result in significant conjugate effects. This explains the

significant difference between the two models found in the current study. The design adopted in the present study is very common in literature, see for example [25] but researchers ignored the conjugate effects. In conclusion, the thin-wall model could be used with certain precautions, i.e. for thin substrates. Additionally, the excellent agreement between the experimental data and the thin-wall model in the present study could be misleading for researchers because the uniform heat flux assumption does not hold true when there is significant conjugate effects.

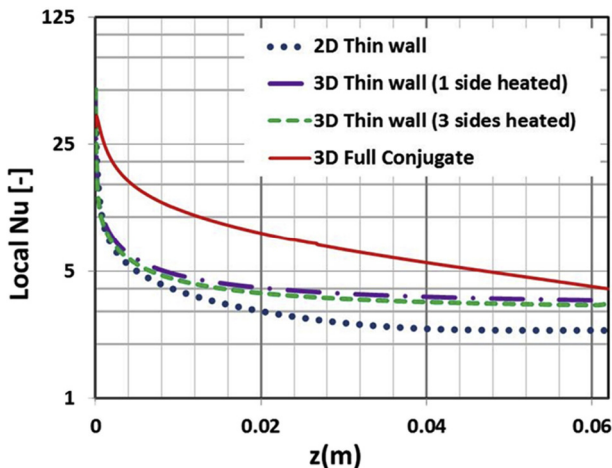


Fig. 15. Variation of local Nusselt number along the channel.

5.2. Multichannel configuration

The chosen approach for multichannel system in this study is based on the simulation results of the single channel configuration. As discussed above, Figs. 12 and 15, clearly show that the heat flux is not uniformly distributed along the channel due to the conjugate effect. Hence, the assumption that the heat flux is uniformly distributed no longer holds true [32]. Therefore, in the multichannel case, it is important to take the conjugate effect into account.

The average velocity and fluid temperature inside the twenty five channels are plotted in Figs. 16 and 17, respectively. The velocity and fluid temperature are averaged along the centre line of each channel. The two figures indicate that the flow distribution depends on the Reynolds number. The flow tends to be uniformly distributed as the Reynolds number decreases. For $Re = 492$, the flow is uniformly distributed along the channels except for the two channels at each side. As the Reynolds number increased above 656, the

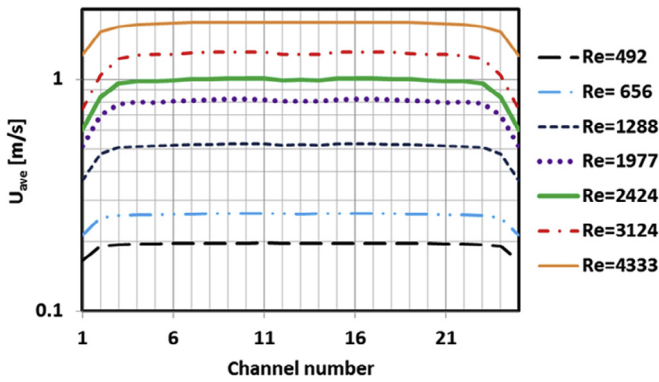


Fig. 16. Velocity average in each channel at different Reynolds number.

flow was uniformly distributed only along the centre channels ($N = 3-23$). This could be due to the large losses at sharp corners of the inlet manifold which increase with Reynolds number. It can be concluded from these figures that the investigated manifold geometry achieved very reasonable flow distribution.

The simulation results of friction factor and heat transfer are compared with experimental results and existing correlations, see Figs. 18 and 19. Fig. 18 depicts that the predicted Fanning friction factor shows a similar trend but with values 38% lower than those calculated by Shah and London [19] in the laminar region and Phillips [33] in the turbulent region. While the values of the predicted friction factor show an excellent agreement with the experimental results for the Reynolds number range 500–1200 and a reasonable agreement up to $Re = 2000$. The predicted values also show that the laminar to turbulent transition jump occurs between $Re = 2000-3000$. The experimental results did not show any transition jump similar to this prediction. The comparison with the prediction after $Re = 2000$ is not conclusive due to lack of experimental data in the transition and turbulent region.

Fig. 19 compares the predicted average Nusselt number (Eq. (25)) values against experimental results (Eq. (19)) and existing correlations. The figure depicts that the experimental Nu is higher than the ones predicted by the current simulation and the Shah and London [19] correlation for developing laminar flow. Also, it increases almost linearly with Reynolds number at a higher rate than in the predictions. The predicted Nu from the current simulation is slightly lower than that the one predicted by Shah and London [19] with a small little dependency on Reynolds number. The deviation between the simulation and Shah and London [19] tends to be larger at low Reynolds numbers. This could be attributed to the effect of axial heat conduction which becomes important as the

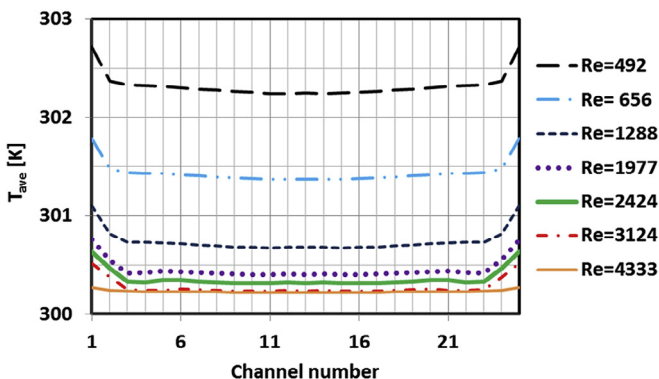


Fig. 17. Temperature average in each channel at different Reynolds number.

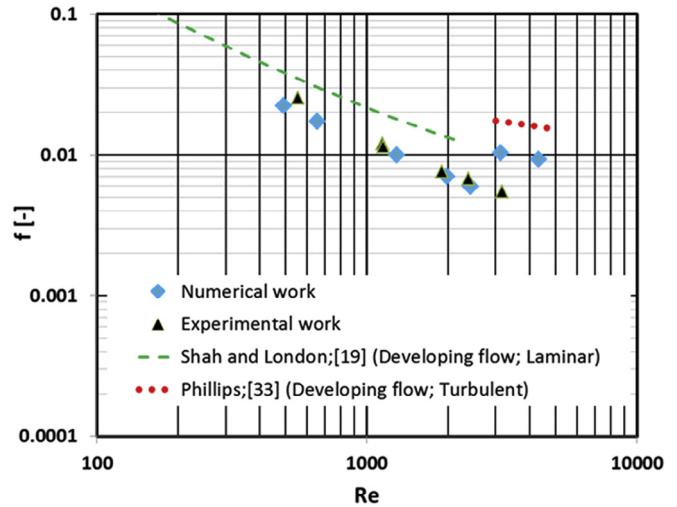


Fig. 18. Comparison of predicted friction factor with experimental results and correlations.

Reynolds number decreases. The axial wall and fluid temperature for multichannel system were depicted in Fig. 14(b). This trend shows a similar trend in single channel system, which might be due to the effect of conjugate heat. Unfortunately, there no data of experimental for local wall temperature and fluid. For the lowest Re , the heat loss due to axial conduction was 1% while at the highest Re the value was 0.3%. This is confirmed in the transition (early turbulent) region, where there is excellent agreement between the experiment and all predictions. The under-prediction of the experimental values in the laminar region could be attributed to the conjugate effects and flow mal-distribution which are not considered in experimental data reduction as discussed before in the single channel configuration.

6. Conclusions

A numerical study has been carried out to investigate single phase heat transfer and fluid flow in a rectangular microchannel using water and R134a as a working fluid in single channel and multi-channel systems, respectively. Four models were investigated namely

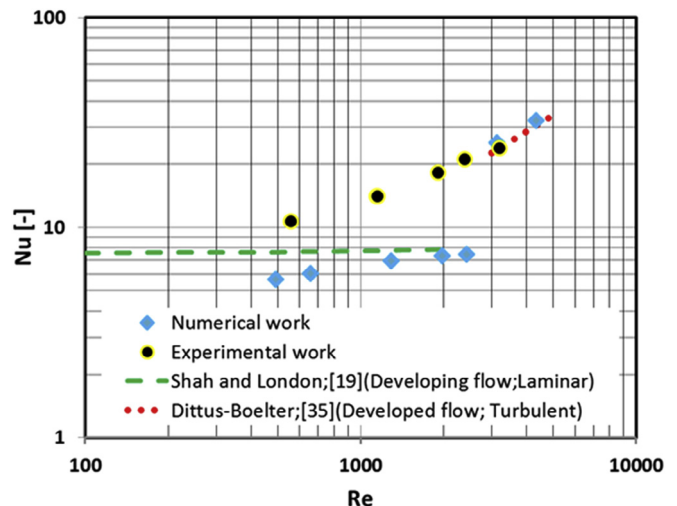


Fig. 19. Comparison of predicted Nusselt with experimental results and correlations.

2D, 3D thin-wall (one side heated), 3D thin-wall (three side heated) and 3D fully conjugated heat transfer model in a single channel system to consider the conjugate effect on heat transfer. In the multichannel system, the conjugate effect was taken into account. The simulations were conducted using FLUENT 14.5. The main conclusions are summarized below:

1. The experimental and numerical results demonstrated that transition from laminar to turbulent occurs at $Re = 1600$ – 2000 .
2. The 3D full conjugate model showed a significant deviation compared to the experimental data indicating significant conjugate effects. The model predicted that the heat flux is not uniformly distributed along the channel. The deviation is attributed to the assumption of uniform heat flux in the experimental data reduction. In order to consider the effect of non uniform heat flux in the experimental data reduction, the local heat flux should be measured accurately, which is very difficult in microchannels. Thus, most researchers assumed uniform heat flux as an approximation. The 3D full conjugate simulation can help determining how much is the error due to the assumption of uniform heat flux boundary condition. For the geometry examined in the present study this error was found to be more than 50% on average.
3. The excellent agreement between the 3D thin-wall model and the experimental data in this study is only due to the fact that they were based on the assumption of uniform heat flux boundary condition, which does not hold true as discussed above. In other words, this agreement does not mean that the simplified 3D thin-wall model is more accurate than the 3D full conjugate model.
4. The predicted friction factor was significantly lower than the prediction by the conventional theory in both laminar and turbulent regions. However, it was found to be in very good agreement with existing experimental results in the laminar region.
5. The inlet manifold with a gradual reduction in flow area exhibited very reasonable performance and uniform flow distribution among the channels.

Nomenclature

A_{ht}	heat transfer area, [m ²]
c_p	specific heat, [J/kg K]
D_h	hydraulic diameter, [m]
f	Fanning friction factor, [–]
G	mass flux, [kg/m ² s]
H_{ch}	channel height, [m]
h_{av}	average heat transfer coefficient, [W/m ² K]
$h_{av,exp}$	average experimental heat transfer coefficient, [W/m ² K]
$h_{av,num}$	average numerical heat transfer coefficient, [W/m ² K]
K_{90}	pressure loss coefficient, [–]
K_c	sudden contraction coefficient, [–]
K_e	sudden enlargement coefficient, [–]
k_f	fluid thermal conductivity, [W/m K]
K_{im}	inlet manifold loss coefficient, [–]
K_{om}	outlet manifold loss coefficient, [–]
k_w	wall thermal conductivity, [W/m K]
L_{ch}	channel length, [m]
\dot{m}	mass flow rate, [kg/s]
N	number of channels, [–]
Nu_{av}	average Nusselt number, $(h_{av}D_h/k_f)$ [–]
$Nu_{av,exp}$	average experimental Nusselt number, [–]
$Nu_{av,num}$	average numerical Nusselt number, [–]
ΔP_{ch}	channel pressure drop, [Pa]
ΔP_c	pressure drop due to sudden contraction, [Pa]
ΔP_e	pressure drop due to sudden expansion, [Pa]
ΔP_{im}	pressure drop in the inlet manifold, [Pa]

ΔP_{meas}	measured pressure drop, [Pa]
ΔP_{loss}	pressure losses, [Pa]
ΔP_{om}	pressure drop in the outlet manifold, [Pa]
p	pressure, [Pa]
P	power, [W]
Pr	Prandtl number, [–] $(\mu C_p/k)$
q_b	base heat flux, [W/m ²]
q_{loss}	rate of heat loss, [W]
q_{rem}	rate of heat removal, [W]
q''	heat flux, [W/m ²]
Re	Reynolds number, $(\rho_f V D_h / \mu_f)$ [–]
T	temperature, [K]
T_w	wall temperature, [K]
T_f	fluid temperature, [K]
$T_{f,av}$	fluid average temperature, [K]
$T_{w,av}$	average wall temperature, [K]
T_i	fluid inlet temperature, [K]
T_o	fluid outlet temperature, [K]
ΔT_{lm}	log-mean temperature difference, [K]
V_p	velocity in the manifold, [m/s]
V_{ch}	velocity inside the channel, [m/s]
v_f	fluid specific volume, [m ³ /kg]
W	width, [m]
W_{ch}	channel width, [m]
x	axial distance, [m]
y	vertical distance, [m]

Greek symbols

θ	diffuser/nozzle conical angle, [°]
μ	viscosity, [kg/m s]
μ_f	fluid viscosity, [kg/m s]
ρ	density, [kg/m ³]
ρ_f	fluid density, [kg/m ³]
σ	area ratio, [–]

References

- [1] D. Tuckerman, R. Pease, High-performance heat sinking for VLSI, IEEE Electron Device Lett. 5 (1981) 126–129.
- [2] P.-S. Lee, G.V. Suresh, D. Liu, Investigation of heat transfer in rectangular microchannels, Int. J. Heat Mass Transfer 45 (2005) 1688–1704.
- [3] S.-S. Hsieh, C.-Y. Lin, C.-F. Huang, H.-H. Tsai, Liquid flow in a micro-channel, J. Micromech. Microeng. 14 (2004) 436–445.
- [4] J.-T. Liu, X.-F. Peng, W.-M. Yan, Numerical study of fluid flow and heat transfer in microchannel cooling passages, Int. J. Heat Mass Transfer 50 (2007) 1855–1864.
- [5] T.M. Harms, M.J. Kazmierczak, F.M. Gerner, Developing convective heat transfer in deep rectangular microchannels, Int. Heat Fluid Flow 20 (1999) 149–157.
- [6] B. Agostini, A. Bontemps, B. Thonon, Effect of geometrical and thermophysical parameters on heat transfer measurements in small diameter channels, Heat Transfer Eng. 27 (1) (2006) 14–24.
- [7] Y.W. Hwang, M.S. Kim, The pressure drop in microtubes and the correlation development, Int. J. Heat Mass Transfer 49 (2006) 1804–1812.
- [8] P. Hrnjak, X. Tu, Single phase pressure drop in microchannels, Int. J. Heat Fluid Flow 28 (2007) 2–14.
- [9] P. Rosa, T. Karayiannis, M. Collins, Single-phase heat transfer in microchannels: the important of scaling effects, Appl. Therm. Eng. 29 (2009) 3447–3468.
- [10] S. Kandlikar, Z. Lu, W. Domigan, A. White, M. Benedict, Measurement of flow maldistribution in parallel channels and its application to ex-situ and in-situ experiment's in PEMFC water management studies, Int. J. Heat Mass Transfer 52 (2009) 1741–1752.
- [11] O. Tonomura, S. Tanaka, M. Noda, M. Kano, S. Hasebe, I. Hashimoto, CFD-based optimal design of manifold in plate-fin microdevices, Chem. Eng. J. 101 (2004) 397–402.
- [12] S. Balaji, S. Lakshminarayanan, Improved design of microchannel plate geometry for uniform flow distribution, Can. J. Chem. Eng. 84 (2006) 715–721.
- [13] M. Pan, X. Shao, L. Liang, Analysis of velocity uniformity in a single microchannel plate with rectangular manifolds at different entrance velocities, Chem. Eng. Technol. 36 (6) (2013) 1067–1074.
- [14] C.-Y. Huang, C.-M. Wu, Y.-N. Chen, T.-M. Liou, The experimental investigation of axial heat conduction effect on the heat transfer analysis in microchannel flow, Int. J. Heat Mass Transfer 70 (2014) 169–173.

- [15] A.G. Fedorov, R. Viskanta, Three-dimensional conjugate heat transfer in the microchannel heat sink for electronic packaging, *Int. J. Heat Mass Transfer* 43 (2000) 399–415.
- [16] M.M. Mansoor, K.-C. Wong, M. Siddique, Numerical investigation of fluid flow and heat transfer under high heat flux using rectangular micro-channels, *Int. Commun. Heat Mass Transfer* 39 (2012) 291–297.
- [17] Mirmanto, D.B.R. Kenning, T.G. Karayiannis, J.S. Lewis, Pressure drop and heat transfer characteristics for single phase developing flow of water in rectangular microchannels, in: 6th European Thermal Sciences Conference (Eurotherm 2012), 2012.
- [18] E.M. Fayyadh, M.M. Mahmoud, T.G. Karayiannis, Flow boiling heat transfer of R134a in multimicrochannels, in: Submitted for the 2nd International Conference on Heat Transfer and Fluid Flow, Barcelona, Spain, July 20–21, 2015.
- [19] R.K. Shah, A. London, Laminar flow forced convection in ducts, in: T.F. Irvine, J.P. Hartnett (Eds), *Advances in Heat Transfer* (Suppl. 1), Academic Press, New York, 1978.
- [20] R. Reimburg, *Thermal Design of Electronic Equipment*, CRC Press, 2000.
- [21] E.J. Shaughnessy, I.M. Katz, J.P. Schaffer, *Introduction to Fluid Mechanics*, Oxford University Press, New York, Oxford, 2005.
- [22] H.W. Coleman, G.W. Steele, *Experimentation and Uncertainty Analysis for Engineering*, second ed., John Wiley and Sons, New York, 1999.
- [23] ANSYS FLEUNT 12.0 User's Guide, ANSYS, Inc.
- [24] W. Qu, I. Mudawar, Experimental and numerical study of pressure drop and heat transfer in a single-phase microchannel heat sink, *Int. J. Heat Mass Transfer* 45 (2002) 2549–2565.
- [25] H. Blasius, Ähnlichkeitsgesetz bei Reibungsvorgängen in Flüssigkeiten, *Forsch. Arb. Ing.-Wes.*, Berlin, 1913.
- [26] J. Zhang, Y. Diao, Y. Zhao, Y. Zhang, An experimental study of the characteristics of fluid flow and heat transfer in the multiport microchannel flat tube, *Appl. Therm. Eng.* 65 (2014) 209–218.
- [27] X. Peng, G. Peterson, B. Wang, Frictional flow characteristics of water flowing through rectangular microchannels, *Exp. Heat Transfer* (1995) 249–264.
- [28] D. Pfund, D. Rector, A. Shekarriz, A. Popescu, J. Welty, Pressure drop measurements in microchannel, *AIChE J.* 46 (8) (2000) 1496–1507.
- [29] G. Iaccarino, A. Ooi, P. Durbin, M. Behnia, Conjugate heat transfer predictions in two-dimensional ribbed passages, *Int. J. Heat Fluid Flow* 23 (2002) 340–345.
- [30] I. Tiselj, G. Hetsroni, B. Mavko, A. Mosyak, E. Pogrebnyak, Z. Segal, Effect of axial conduction on the heat transfer in microchannels, *Int. J. Heat Mass Transfer* 47 (2004) 2551–2565.
- [31] M.K. Moharana, P.K. Singh, S. Khandekar, Optimum Nusselt number for simultaneously developing internal flow under conjugate conditions in a square microchannel, *J. Heat Transfer* 134 (2012) 1–10.
- [32] A. Bansode, S. Patel, T.R. Kumar, B. Muralidhar, T. Sundararajan, S.K. Das, Numerical simulation of effects of flow maldistribution on heat and mass transfer in a PEM fuel cell stack, *Heat Mass Transfer* 43 (2007) 1037–1047.
- [33] R.J. Phillips, Forced-convection, Liquid-cooled, Microchannel Heat Sinks (MS Thesis), Department of Mechanical Engineering, Cambridge, 1987, p. 70.
- [34] A. Bejan, *Convection Heat Transfer*, John Wiley & Son, Inc, New Jersey, 2004.
- [35] F.W. Dittus, L.M.K. Boelter, vol. 2/13, *Heat Transfer in Automobile Radiators of Tubular Type*, Univ. California Berkeley, Publ. Eng., 1930, pp. 443–461.